American Journal of Optics and Photonics
2022; 10(4): 23-28
http://www.sciencepublishinggroup.com/j/ajop
doi: 10.11648/j.ajop.20221004.11
ISSN: 2330-8486 (Print); ISSN: 2330-8494 (Online)

Monolithic Integration of a Multiwavelength Laser Array Associated with SBG Semiconductor Lasers

Renjia Guo[1, *], Jing Wu[2], Dikui Mei[1], Ping Wang[3], Lili Liu[4], Jichu Dong[5]

[1]School of Physics and Electronic Engineering, Jiangsu Intelligent Optoelectronic Devices and Measurement and Control Engineering Research Center, Yancheng Teachers University, Yancheng, China

[2]School of Biological Science and Technology, Yangzhou University, Yangzhou, China

[3]Yancheng Tongji Automotive Parts Limited Corporation, Yancheng, China

[4]Jiangsu Tongji Analytical Instrument Limited Corporation, Yancheng, China

[5]Yancheng Jinzhou Machinery Manufacturing Limited Corporation, Yancheng, China

Email address:

guorj@yctu.edu.cn (Renjia Guo), 704780906@qq.com (Jing Wu), mei_dikui@163.com (Dikui Mei), 202534523@qq.com (Ping Wang), 4822216@qq.com (Lili Liu), 170372780@qq.com (Jichu Dong)

[*]Corresponding author

To cite this article:

Renjia Guo, Jing Wu, Dikui Mei, Ping Wang, Lili Liu, Jichu Dong. Monolithic Integration of a Multiwavelength Laser Array Associated with SBG Semiconductor Lasers. *American Journal of Optics and Photonics*. Vol. 10, No. 4, 2022, pp. 23-28. doi: 10.11648/j.ajop.20221004.11

Received: November 6, 2022; **Accepted**: November 21, 2022; **Published**: November 29, 2022

Abstract: There are strong demands of monolithically integrated photonic components for future high capacity optical networks such as those for data center, fifth-generation fronthaul or wavelength-division multiplexing systems. Monolithically integrated multiwavelength laser array (MLA) is a potential photonic component used in the above applications. The monolithically integrated MLA associated with sampled Bragg grating (SBG) semiconductor lasers is proposed and studied here. It is shown in the results that a controllable phase shift can be introduced into the central part of the cavity to tune the lasing wavelength. The effective refractive index along the phase-shift-controlled (PSC) parts was different from those of the side parts with the different currents injected into the PSC parts and the side parts. So the optical path length along the PSC part changed for the lasing wavelength. In other words, an appropriate distributed phase shift along the PSC part could be introduced accordingly. Besides, it is found in the results that the longitudinal photon density distribution of the proposed structure is much flatter than that of the λ/4 phase-shift structure. Hence, the longitudinal spatial hole burning (SHB) is reduced more effectively. The single longitudinal mode (SLM) stability is better than that of the common λ/4 phase-shift structure at high injection currents accordingly. A twelve-channel SBG MLA with 50-GHz wavelength spacing was fabricated in the experiment. The channel frequency ranges from 192.70 THz to 192.15 THz. Its operation at designed wavelengths was demonstrated. High side mode suppression ratios (SMSRs) of all channels over 57 dB were observed as well. This paves the way for a compact and cost-efficient light source for large-scale photonic integrated circuit devices.

Keywords: Multiwavelength Laser Array, Sampled Bragg Grating, Spatial Hole Burning

1. Introduction

Distributed feedback (DFB) semiconductor multiwavelength laser arrays (MLAs) have been widely used in optical communication systems, photonic integral circuit, photoelectric sensing, and photoelectric signal operation [1-9]. The most common type is the λ/4 phase-shift DFB MLA operating in the single longitudinal mode (SLM) and the lasing wavelength is controllable by the design of grating structure [10-14]. However, the non-uniformity of the carrier density distribution may become very serious when it works at high injection currents. Such non-uniformity may degrade the mode stability through changing the effective refractive index, which leads to multimode operation. It is known that the deterioration of the SLM is mainly caused by the longitudinal spatial hole burning (SHB) effect [15-17]. Meanwhile, the SLM is also influenced by the minor damage of anti-reflection films at both facets [18]. A lot of special structures have been proposed to

achieve good SLM performance, such as the chirp-modulated structure, the corrugation-pitch-modulated (CPM) structure, the multiple phase shifts structure, the λ/8 phase-shift structure [19, 20]. However, these special structures are always complex and not easy to fabricate. The electron beam lithography (EBL) is a practical method to write the complex nano-structures, but it is time-consuming and expensive.

Recently, a sampled Bragg grating (SBG) has been widely used, which formed by traditional holographic exposure and lithography. MLA can be easily fabricated by designing sampled period of the order of micrometers [21-24]. The sampled Bragg grating can be used to tune Bragg wavelength of the order of nanometers. So SBG shows great potential in MLA fabrication.

In this work, a three-electrode SBG MLA with phase-shift-controlled (PSC) part has been proposed and studied. It is shown that the longitudinal photon density distribution of the proposed SBG MLA is much flatter than that of a λ/4 phase-shift DFB MLA. The proposed SBG MLA is one of the promising devices to suppress the spatial hole burning effect. Because the carrier density distribution is controlled by the injection currents via the three separated electrodes, the phase-shift can be tuned by changing the injection currents. With an appropriate phase-shift, the proposed SBG MLA maintains the SLM operation. The controllability of the carrier density distribution in the proposed SBG MLA is also essential for obtaining a tunable wavelength range. A twelve-channel SBG MLA with 50-GHz wavelength spacing is fabricated. Its operation at designed wavelengths is demonstrated as well.

2. Principle and Design

In the SBG MLA, the corrugation of grating gives the feedback. Because only the SLM behavior of the SBG MLA is of interest, we suppose that there is merely one mode oscillates. The relationship between the injection current and the carriers can be expressed as

$$\frac{\mathrm{I}(z)}{ed} = AN_1(z) + BN_1^{\ 2}(z) + CN_1^{\ 3}(z) + v_g g(z) N_2(z) \qquad (1)$$

where I is the injection current, e is the electronic charge, d is the active layer thickness, N_1 is the carrier density, A is equal to $1/\tau$, where τ is the linear recombination time, B is the bimolecular recombination coefficient, C is Auger recombination coefficient, vg is the group velocity, N_2 is the photon density in the active region and g is power gain which can be expressed as

$$\mathrm{g}(N_1(z)) = A_0(N_1(z) - N_3(z)) \qquad (2)$$

where A_0 is the differential gain, N_3 is the transparency carrier density. Then the effective refraction index of the wavelength λ would be

$$n_e(\lambda) = n_e^{\ 0}(\lambda) - \frac{\lambda}{4\pi} A_0 \Gamma \alpha_H N_1 \qquad (3)$$

where $n_e^{\ 0}(\lambda)$ is the effective refraction index of the wavelength λ when there is no carriers, Γ is the confinement factor and α_H is the line-width enhancement factor.

Figure 1 shows the schematic illustration of a proposed SBG MLA with three electrodes which are equally separated. Then the currents I_s and I_p are injected into the side part and PSC part of proposed SBG MLA, respectively. Because the two side parts are identical, the current injected into the left side part or the right one is the same to each other, which equals to $I_s/2$. We assume that facets at front and back are AR-coated.

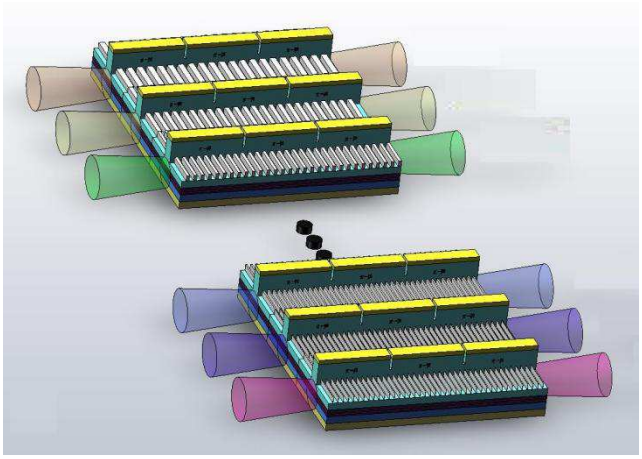

Figure 1. *The schematic illustration of a proposed SBG MLA.*

When the currents are injected into the proposed SBG MLA, there would be band-filling, band-gap shrinkage and free-carrier plasma effect [25]. In this work, the grating along the resonant cavity is uniform and the period of the grating is Λ. The effective refractive index along the resonant cavity is the same when there is no current injected. When the currents are injected into the electrodes, the effective refractive index would change accordingly. If there is a subtle distinction between the effective refractive indexes of the PSC part and the side parts, a distributed phase-shift is introduced in the whole PSC part. The distributed phase-shift can be expressed as:

$$\theta = \frac{2\pi(\overline{n}_s - \overline{n}_c)L_2}{\overline{n}_s \Lambda} \qquad (4)$$

Where $\overline{n}_s$ and $\overline{n}_c$ are the average effective refractive index of the side parts and the PSC part.

3. Results and Discussion

The characteristics of the proposed SBG MLA are studied using the transfer matrix method (TMM) [26]. From each transfer matrix, the carrier concentration, photon density, refractive index and amplitude gain can be evaluated. The characteristic of the proposed SBG MLA is determined by passing the values from one transfer matrix to the next transfer matrix.

Table 1. *List of parameter values used in the simulation.*

Parameters	Data
Cavity length (l)	600 μm
Effective refractive index	3.17
Group index	3.7
Line width enhancement factor	3.5
Duty cycle	0.5
Constraint factor	0.3
Carrier density on base	0.0012 cm^{-3}
Effect of differential quantum	0.015
Kappa (κ)	3.0 mm^{-1}
$\kappa \times l$	1.8

In this model, the period of the grating is 246.08 nm. The length of the laser cavity is 600 μm. The modulated depth of the refractive index is about 0.0015. Other parameters used in the simulation are listed in the Table 1.

The simulation in which the total current is 130 mA constant is called the Simulation-A. The simulation in which the side current is 30 mA constant and the current of the PSC part changed from 40 to 70 mA is called the Simulation-B.

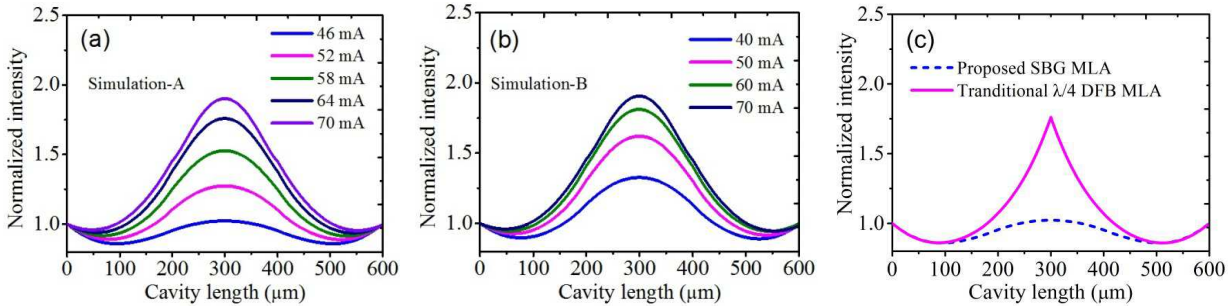

Figure 2. *The normalization photon intensity distributions along the cavity for (a) Simulation-A, (b) Simulation-B and (c) a λ/4 phase-shifted structure with current 130 mA and proposed SBG MLA under Is = 84 mA and Ip = 46 mA.*

It is found in the Figure 2a that I_p increased from 46 mA to 70 mA. $I_s/2$ decreased from 42 mA to 30 mA accordingly. The photon distribution although the cavity became steeper when I_p became higher. In Figure 2b, $I_s/2$ is 30 mA constant. I_p increased from 40 mA to 70 mA. The total current increased from 100 mA to 130 mA accordingly. It is also found that the photon distribution although the cavity became steeper when I_p became higher. By comparing Figure 2a with Figure 2b, it is found that the photon distribution is the same when I_p is 70 mA. With I_p decreased, the photon distribution became flatter much faster of Simulation-A than that of Simulation-B. It is because that $I_s/2$ increased when I_p decreased in Simulation-A. However, $I_s/2$ is 30 mA constant when I_p decreased in Simulation-B. The difference between I_p and $I_s/2$ became smaller much faster of Simulation-A than that of Simulation-B.

When compared with a λ/4 phase-shifted DFB MLA in Figure 2c, without a peak in the center, the photon intensity of the proposed SBG MLA is much flatter. The reason is that the photon is drawn by the distributed phase-shift of the PSC part. It can help to reduce the highly concentrated photon and smooth the photon distribution along the cavity in the PSC part. It is of importance that the proposed SBG MLA can reduce the SHB effect more effectively. The smaller the difference between the current of the side parts and the PSC part, the flatter the photon intensity distribution along the cavity of the proposed SBG MLA is (Figure 2a, b).

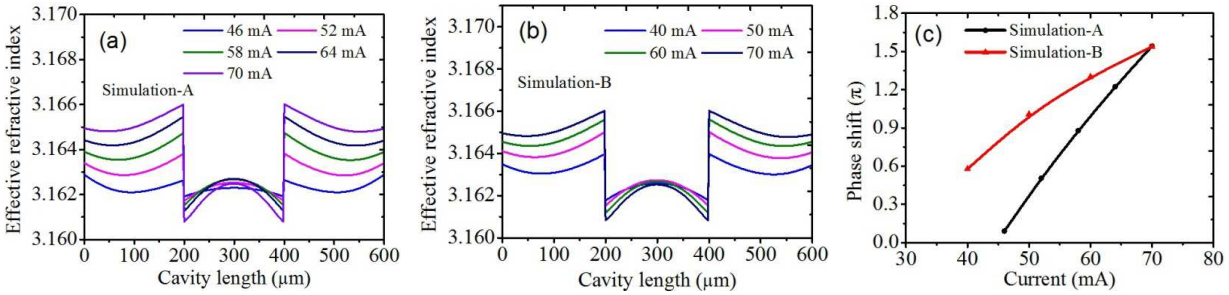

Figure 3. *The effective refractive index distributions along the cavity of proposed SBG MLA in the (a) Simulation-A, (b) Simulation-B and (c) The corresponding phase-shifts of the proposed SBG MLA.*

It is found in the Figure 3a that I_p increased from 46 mA to 70 mA. $I_s/2$ decreased from 42 mA to 30 mA accordingly. The effective refractive index distribution although the cavity became more precipitous when I_p became higher. In Figure 3b, $I_s/2$ is 30 mA constant. I_p increased from 40 mA to 70 mA. The total current increased from 100 mA to 130 mA accordingly. It is also found that the effective refractive index distribution although the cavity became more precipitous when I_p became higher. By comparing Figure 3a with Figure 3b, it is found that the effective refractive index distribution is the same when I_p is 70 mA. With I_p decreased, the effective refractive index distribution became flatter much faster of Simulation-A than that of Simulation-B. It is because that $I_s/2$ increased when I_p decreased in Simulation-A. Howerve, $I_s/2$

is 30 mA constant when I_p decreased in Simulation-B. The difference between I_p and $I_s/2$ became smaller much faster of Simulation-A than that of Simulation-B.

In order to keep the SLM operation, there should be difference between the injection current of the PSC part and those of the side parts to obtain a suitable phase shift. The horizontal axis is the bias current injected into the PSC part in Figure 3c. The slope efficiency of the curve is about 0.06 and 0.03 π/mA according to the current of the PSC part in the Simulation-A and the Simulation-B, respectively. With the increase of the PSC currents in the Simulation-A, the side currents decrease, but the side currents are constant in the Simulation-B, it is easy to understand the slope efficiency in the Simulation-A is about twice than that in the Simulation-B. The refractive index and the phase-shift is almost uniformly changed (Figure 3c) when the current of the PSC part increased in Simulation-A, but the refractive index and the phase-shift is non-uniformly changed (Figure 3c) in the Simulation-B. That is to say, in the Simulation-B, the changing rate of the effective refractive index difference inside and outside the PSC part decreased when the total current increased.

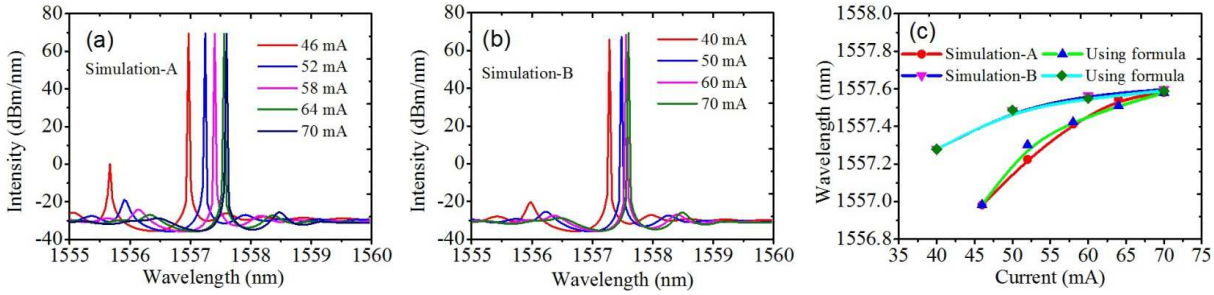

Figure 4. *The simulated spectra of proposed SBG MLA in the (a) Simulation-A, (b) Simulation-B and (c) The correspond lasing wavelength of the proposed SBG MLA under different current injected into the PSC part.*

Figure 4a, b are the spectra of proposed SBG MLA which are simulated in the Simulation-A and the Simulation-B, respectively. It is found in the Figure 4a that I_p increased from 46 mA to 70 mA. $I_s/2$ decreased from 42 mA to 30 mA accordingly. The lasing wavelength became red shifted when I_p became higher. In Figure 4b, $I_s/2$ is 30 mA constant. I_p increased from 40 mA to 70 mA. The total current increased from 100 mA to 130 mA accordingly. It is also found that the lasing wavelength also became red shifted when I_p became higher. By comparing Figure 4a with Figure 4b, it is found that the lasing wavelength is the same when I_p is 70 mA. With I_p decreased, the lasing wavelength became red shifted much faster of Simulation-A than that of Simulation-B. The tuning ranges are 0.6 nm and 0.39 nm of Simulatiion-A and Simulation-B respectively. It is because that $I_s/2$ increased when I_p decreased in Simulation-A. Howerve, $I_s/2$ is 30 mA constant when I_p decreased in Simulation-B. The difference between I_p and $I_s/2$ became smaller much faster of Simulation-A than that of Simulation-B.

From the spectra it can be speculate that when the injection current of the PSC part is close to the side currents, the proposed laser has two lasing modes. With the increase of the difference between the currents of the PSC part and the side parts, the proposed SBG MLA turns into the SLM. In our simulation, when the phase shift changed from π/2 to 3π/2 (Figure 3c), the proposed laser maintained the good SLM operation (Figure 4a, b).

The wavelength can be expressed as:

$$\lambda \approx \lambda_1 + k_1\sqrt{\frac{\theta-\theta_1}{\pi}} \tag{5}$$

where λ_1 is the lasing wavelength and θ_1 is the phase shift when the current of the PSC part is 46 mA in the Simulation-A and 40 mA in the Simulation-B, respectively. k_1 is 0.7 nm in the Simulation-A and 0.45 nm in the Simulation-B, respectively.

In Figure 4c, the horizontal axis is marked by the bias current injected into the PSC part. With an appropriate phase-shift in the simulation, such as, from π/4 to 7π/4 (Figure 2b), the lasing wavelength could be tuned from 1556.98 to 1557.58 nm in the Simulation-A. By using the Equation 5, the wavelength could be tuned from 1556.98 to 1557.58 nm. The tunable ranges were both about 0.6 nm.

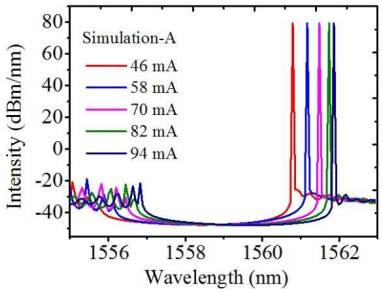

Figure 5. *The spectra of proposed SBG MLA under the total current is 130 mA when refractive index modulated depth is 0.01.*

As a matter of fact, in an actual SBG MLA, the modulated depth of the refractive index can be higher than 0.01, corresponding to the coupling coefficient κ being to about 20 mm^{-1}. When κ is 20 mm^{-1} and the total current is 130 mA, the lasing wavelength could be tuned from 1560.80 to 1561.87 nm in the Simulation-A (Figure 5) and the tunable range is about 1.1 nm.

By comparing Figure 5 with Figure 4a and Figure 4b, it is

found that the lasing wavelength tuning range became bigger with the modulated depth of the refractive index became higher. It is because that the Bragg wavelength became bigger when the modulated depth of the refractive index became higher. Moreover, if there is the thermal effect, the red-shift of the thermal effect would help to expand the tunable range of the lasing wavelength.

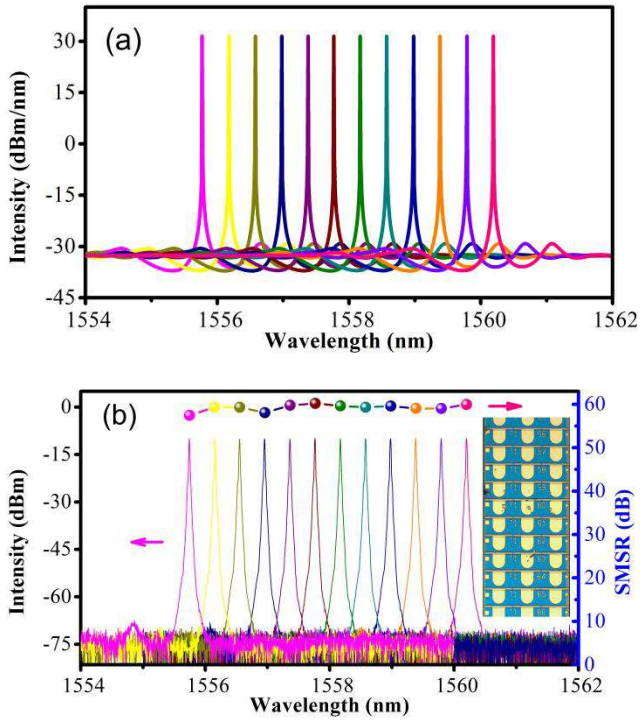

Figure 6. *The spectra of proposed SBG MLA in the (a) simulation and (b) experiment. The inset gives the microscope image of the proposed SBG MLA chip.*

The simulated spectra of the proposed SBG MLA are plotted in Figure 6a. The same performance is obtained for the 12 lasing wavelengths. The channel spacing is 50 GHz. The results show that SBG MLA would provide high performance. The simulated result demonstrates the excellent wavelength precision that can be achieved with SBG.

In the experiment, a 600 μm SBG MLA based on electrically controlled was placed on a smooth copper surface at room temperature of 25°C. The overlapping spectra with channel spacing of 50 GHz are studied (Figure 6b). There are 12 channels in total. The channel frequency ranges from 192.70 THz to 192.15 THz, and the corresponding wavelengths range from 1555.747 nm to 1560.200 nm. High SMSRs of all channels over 57 dB were observed as well.

By comparing Figure 6a and Figure 6b, it is found that the experimental results agree with the simulation results very well. The proposed MLA operated at the designed wavelengths was achieved in the experiment. The yield of laser in the propose MLA is very high. It is benefited from the distributed phase shift in the PSC part.

4. Conclusion

The MLA associated with SBG semiconductor lasers is proposed and studied. The proposed SBG MLA was fabricated with the uniform grating obtained from the common two beam interference. With changing the currents injected into the side and PSC parts, arbitrary phase shift can be introduced into this proposed SBG MLA. It is demonstrated that the internal longitudinal photon density distribution of the proposed SBG MLA is much flatter than that of a traditional λ/4 phase-shift DFB MLA. Hence, the longitudinal SHB effect is considerably reduced and the proposed SBG MLA has good SLM performance. Also the lasing wavelength could be tuned by controlling the amounts or ratio of the injection currents into the side and PSC parts. A twelve-channel SBG MLA with 50-GHz wavelength spacing is fabricated. Its operation at designed wavelengths is demonstrated. High SMSRs of all channels over 57 dB were observed as well.

Acknowledgements

The authors would like to acknowledge the support from the National Natural Science Foundation of China (61904157, 61904158, 11847161), Joint Project of Industry University Research of Jiangsu Province (BY2020630), Jiangsu College Student Innovation and Entrepreneurship Training Program (202110324001Z, 202110324027Y). The authors also thank Prof. Yating Zhou for fruitful discussion of designing the grating. The authors thank Prof. Xiangfei Chen for valuable discussion of the sampled Bragg grating.

References

[1] W. Bogaerts, D. Perez, J. Capmany, et al. Programmable photonic circuits. Natrue, vol. 586, pp. 207-216, 2020. doi: 10.1038/s41586-020-2764-0.

[2] A. Atabaki, S. Moazeni, Pavanello, et al. Integrating photonics with silicon nanoelectronics for the next generation of systems on a chip. Nature, vol. 556, pp. 349-354, 2018. doi: 10.1038/s41586-018-0028-z.

[3] T. Yamaoka, T. Tsuchizawa, F. Koyama, et al. Directly modulated membrane lasers with 108 GHz bandwidth on a high-thermal-conductivity silicon carbide substrate. Nature Photonics, vol. 15, pp. 28-35, 2021. doi: 10.1038/s41566-020-00700-y.

[4] Z. Wang, B. Tian, Pantouvaki, et al. Room-temperature InP distributed feedback laser array directly grown on silicon. Nature Photonics, vol. 9, pp. 837-842, 2015. doi: 10.1038/nphoton.2015.199.

[5] A. Li, J. Wang, C. Sun, et al. 1.3 μm 10-wavelength laterally coupled distributed feedback laser array with high-duty-ratio gratings. Physica Status Solidi A, vol. 216, no. 1, pp. 1800490, 2019. doi: 10.1002/pssa.201800490.

[6] S. Ryu, J. Kim. An asymmetric sampled grating laser and its application to multi-wavelength laser array. Electronics and Telecommunications Research Institute Journal, vol. 24, no. 5, pp. 341-348, 2002. doi: 10.4218/etrij.02.0102.0502.

[7] X. Zou, F. Zou, Z. Cao, et al. A multifunctional photonic integrated circuit for diverse microwave signal generation, transmission, and processing. Laser Photonics Reviews, vol. 13, no. 6, pp. 1800240, 2019. doi: 10.1002/lpor.201800240.

[8] C. Arellano, Mingaleev, E. Sokolov, et al. The power of circuit simulations for designing photonic integrated circuits. Concurrency and Computation: Practice Experience, vol. 26, no. 15, pp. 2518-2529, 2013. doi: 10.1002/cpe.3335.

[9] J. Zhang, C. Sun, B. Xiong, et al. Surface grating fabrication by inductively coupled plasma dry etching for InP-based photonic integrated circuits. Physica Status Solidi A, vol. 215, no. 18, pp. 1800406, 2018. doi: 10.1002/pssa.201800406.

[10] S. Dhoore, A. Koninger, R. Meyer, et al. Electronically tunable distributed feedback (DFB) laser on Silicon. Laser Photonics Reviews, vol. 13, no. 3, pp. 1800287, 2019. doi: 10.1002/lpor.201800287.

[11] H. Cantu, A. Mckee, P. Ivanov, et al. The effect of detuned wavelength in the dynamic performance of distributed feedback lasers operating at O band and C band. Microwave and Optical Technology Letters, vol. 62, no. 4, pp. 1466-1470, 2020. doi: 10.1002/mop.32206.

[12] H. Kim, G. Khinda, J. Jules, et al. Modeling of yield, slope efficiency, and spectra of multisegment distributed feedback lasers. Microwave and Optical Technology Letters, vol. 60, no. 1, pp. 25-31, 2018. doi: 10.1002/mop.30912.

[13] S. Jang, C. Yeo, J. Yu, et al. 1.55-μm DFB lasers with narrow ridge stripe and second-order metal surface gratings by holographic lithography. Physica Status Solidi A, vol. 207, no. 8, pp. 1982-1987, 2010. doi: 10.1002/pssa.200925353.

[14] J. Zhang. The effect of spatial hole burning on FM response in DFB laser diodes. Microwave and Optical Technology Letters, vol. 4, no. 9, pp. 372-375, 1991. doi: 10.1002/mop.4650040912.

[15] C. Fernandes. Impact of structural changes in the corrugation on the DFB laser characteristics. Microwave and Optical Technology Letters, vol. 25, no. 5, pp. 352-355, 2000. doi: 10.1002/mop.17302.

[16] H. Lee, H. Kim, B. Kim, et al. Distributed feedback lasers with refractive-index-modulated upper cladding layer of the grating for reducing the spatial hole-burning effect. Microwave and Optical Technology Letters, vol. 26, no. 3, pp. 173-176, 2000. doi: 10.1002/mop.12302.

[17] P. Rauter, F. Capasso. Multi-wavelength quantum cascade laser arrays. Laser Photonics Reviews, vol. 9, no. 5, pp. 452-477, 2015. doi: 10.1002/lpor.201500095.

[18] P. Mols, P. Kuindersma, W. Es-Spiekman, et al. Yield and device characteristics of DFB lasers: statistics and novel coating design in theory and experiment. IEEE Journal of Quantum Electronics, vol. 25, no. 6, pp. 1303-1313, 1989. doi: 10.1109/3.29261.

[19] K. Torgil, N. Stefan, K. Tiina, et al. Investigation on the spectral characteristics of DFB lasers with different grating configurations made by electron-beam lithography. Journal of Lightwave Technology, vol. 11, no. 9, pp. 1405-1415, 1993. doi: 10.1109/50.241930.

[20] M. Okai, N. Chinone, H. Taira, et al. Corrugation-pitch-modulated phase-shifted DFB laser. IEEE Photonics Technology Letters, vol. 1, no. 8, pp. 200-201, 1989. doi: 10.1109/68.36041.

[21] Y. Shi, S. Li, X. Chen, et al. High channel count and high precision channel spacing multi-wavelength laser array for future PICs. Scientific Reports, vol. 4, pp. 7377, 2014. doi: 10.1038/srep07377.

[22] S. Tang, J. Lu, J. Wang, et al. Integrated buried heterostructure DFB laser array for WDM systems based on reconstruction equivalent chirp technique. Microwave and Optical Technology Letters, vol. 57, no. 6, pp. 1278-1281, 2015. doi: 10.1002/mop.29075.

[23] Z. Sun, R. Xiao, Z. Su, et al. High single-mode stability tunable in-series laser array with high wavelength-spacing uniformity. Journal of Lightwave Technology, vol. 38, no. 21, pp. 6038-6046, 2020. doi: 10.1109/jlt.2020.3005828.

[24] J. Lu, S. Liu, Q. Tang, et al. Multi-wavelength distributed feedback laser array with very high wavelength-spacing precision. Optics Letters, vol. 40, no. 22, pp. 5136-5139, 2015. doi: 10.1364/ol.40.005136.

[25] B. Brian, S. Richard, A. Jesus. Carrier-induced change in refractive index of InP, GaAs and InGaAsP. IEEE Journal of Quantum Electronics, vol. 26, no. 1, pp. 113-122, 1990. doi: 10.1109/3.44924.

[26] M. Toshihiko, G. Jan. Transfer matrix analysis of the amplified spontaneous emission of DFB semiconductor laser amplifiers. IEEE Journal of Quantum Electronics, vol. 24, no. 8, pp. 1507-1518, 1988. doi: 10.1109/3.7077.